Received 12 October 2020; accepted 26 October 2020. Date of publication 2 November 2020; date of current version 7 December 2020.

*Digital Object Identifier 10.1109/OJCOMS.2020.3034747*

# Energy-Constrained Uncoordinated Multiple Access for Next-Generation Networks

**F. BABICH (Senior Member, IEEE), G. BUTTAZZONI (Member, IEEE), F. VATTA (Member, IEEE), AND M. COMISSO (Member, IEEE)**

Department of Engineering and Architecture, University of Trieste, 34127 Trieste, Italy

CORRESPONDING AUTHOR: F. BABICH (e-mail: babich@units.it)

This work was supported in part by the Italian Ministry of University and Research within project FRA 2018 (University of Trieste, Italy) "UBER-5G: Cubesat 5G networks—Access layer analysis and antenna system development."

**ABSTRACT** This article analyzes the performance of a distributed joint power/packet diversity random access scheme in the presence of energy requirements. In particular, the two main approaches separately developed in the recent years for exploiting the Interference Cancellation (IC) capabilities of modern receivers, that is, Non-Orthogonal Multiple Access (NOMA) and Packet Repetition (PR), are firstly compared and then combined by imposing a constraint on the total available power. This constraint, which is alternative to the commonly adopted one based on the maximum power allowed for a transmission, results much more practical, since it enables to better infer the energy efficiency of a scheme, be it a pure NOMA, PR or combined NOMA/PR one. Both theoretical derivations and numerical simulations are carried out to evaluate the success probability and the throughput of the considered schemes by accounting for evolved reception criteria and different fading scenarios. Furthermore, the influence of several nonidealities, including imperfect IC and packet overhead, is discussed together with the impact of the system parameters, such as the user rate, the average signal to noise ratio, and the number of slots that compose a random access frame.

**INDEX TERMS** Random access, slotted Aloha, NOMA, packet diversity, energy constraints.

## I. INTRODUCTION

RANDOM access represents a fundamental issue for all kinds of networks that cannot rely on a centralized authority for managing the communications [1]–[4]. Its importance will further grow in the forthcoming fifth and sixth-generation (5G/6G) systems, whose final aim will be that of creating a pervasive space/terrestrial wireless scenario implementing the Internet of Things (IoT) paradigm. To this purpose, 5G/6G technologies will have to reliably support a large number of possible distributed applications, covering management, automation, safety, and security services, whose simultaneous execution will generate sporadic and heterogeneous traffic.

### A. RELATED WORK

Current 2-4G cellular networks manage the distributed load by adopting the well known Slotted Aloha (SA) protocol [5], for which several extensions, suitable for the more challenging 5G/6G scenario, have been proposed. The SA performance may be in fact significantly improved by introducing energy diversity and Interference Cancellation (IC), whose combination enables to design different Non-Orthogonal Multiple Access (NOMA) schemes [6]–[14]. More precisely, the NOMA concept consists in allowing a set of users, which rely on the same modulation and code rate, to transmit using different energy levels selected in a set of $L$ elements. This concept may be used both in centralized and distributed scenarios. In a centralized system, such as a cellular one, the coordinating authority, represented by the base station, assigns the different levels to the different users. Instead, in a distributed system, each user randomly selects its level by knowing the allowed ones, but not knowing those selected by the other users. In particular, the levels are chosen so that, if at most $L$ users send their packets in a given slot using different levels, all the packets can be decoded. Beside NOMA, another approach has been developed in the last years for increasing the SA throughput. This approach, which combines Packet Repetition (PR) and IC, relies on

the transmission of a certain number $M$ of replicas of a packet [15]–[19]. Two fixed repetitions are adopted in the Contention Resolution Diversity SA (CRDSA) protocol [15], while a random number of them is used in the Irregular Repetition SA (IRSA) scheme [16], already included in the last update of the DVB-RCS2 standard [17], and in its prioritized extension [18]. A coded strategy is alternatively adopted in the Coded SA (CSA) algorithm [19], where the packets are firstly divided into segments and subsequently encoded. Some useful proposals have also investigated the combination of NOMA and PR to jointly exploit energy and packet diversities [20]–[23]. In particular, in [20], the benefits of PR in a NOMA scheme are analyzed by introducing a multichannel SA system, while, in [21] and [22], the NOMA/CRDSA scheme is specifically discussed and an analytical expression for the packet error probability is derived. The NOMA/IRSA case is instead addressed in [23], where the degree-distributions originally presented in [16] are recalculated for the joint scheme.

The above studies have highlighted the benefits of combined NOMA/PR strategies in an ideal scenario, but their actual applicability to real contexts requires further considerations. Firstly, the impact of imperfect IC and unideal power control should be better quantified [9], since the residual interference and the fading effects may significantly affect the evolution of the IC process. Secondly, for cost and safety reasons, ultra-dense 5G/6G networks will be characterized by stringent energy saving constraints [24], [25], whose influence on NOMA/PR strategies has not been even deeply addressed. Thirdly, the detection criterion should properly match the behavior of a real receiver, in which a successful reception does not occur only for the single uncollided or cleaned (after IC) slot (*single-slot* erasure model). In a practical receiver, in fact, even a collision may lead to decodable packets, as long as the Signal to Interference-plus-Noise Ratio (SINR) of one of them lies beyond the reception threshold [26]–[28]. Besides, when PR schemes are used, suitable headers must be added to each packet replica for enabling the receiver to identify, within the Random Access Frame (RAF), the positions of the other replicas of the same packet [29]. These headers enable, on one hand, the cancellation of the replicas of an already decoded packet, and, on the other hand, the study of more evolved *multi-slot* capture models, such as Chase combining, in the presence of PR, or joint decoding, in the presence of incremental redundancy [30]–[34]. Preliminary simulations concerning the impact of the reception model and of the energy requirement on the performance of a combined power/packet diversity scheme have been presented in [35], but ideally assuming perfect IC and absence of fading.

### B. CONTRIBUTION

In light of these considerations, this article investigates the performance of distributed joint NOMA/PR schemes under total power constraints, adopting both single- and multi-slot detection techniques in the presence of Rayleigh fading and imperfect IC. To this aim, the NOMA energy levels and the transmission power of each packet replica are analytically derived in agreement with the rate and the residual interference due to unideal IC. Subsequently, tight upper bounds on the success probability in slow and fast fading scenarios are theoretically estimated for different reception criteria, including the single-slot erasure model and the multi-slot capture ones represented by Chase combining and joint packet decoding. In particular, closed-form expressions for the success probability of a NOMA scheme are obtained for any number of energy levels in a fading-less channel. All theoretical results are validated by extensive Monte Carlo simulations, which are also carried out to investigate the dependance of the throughput from the average Signal to Noise Ratio (SNR) and the header carried by each replica.

This article is organized as follows. Section II describes the energy design. Section III derives the upper bounds on the success probability. Section IV discusses the obtained results. Finally, Section V summarizes the main conclusions.

## II. ENERGY LEVEL DESIGN

Consider a distributed wireless network in which $H$ contending users send packets to a common destination. The packet arrival is described by a Poisson process and the time domain is subdivided into RAFs of $K$ slots. Each user, assumed frame- and slot-synchronous, sends at most one packet in each RAF by randomly selecting, among the $K$ slots, those in which $M$ replicas or $M$ encoded segments are inserted. The term 'segment' is from now on adopted in general to identify the possibility of including in the analysis either repetition or incremental redundancy, in which the content of a slot may be designed to be individually decodable. In particular, the pure SA and NOMA schemes [6], are characterized by $M = 1$, since they do not use repetition. Instead, the pure CRDSA and the joint NOMA/CRDSA schemes [15], are characterized by $M = 2$, while, in the pure IRSA and the joint NOMA/IRSA ones, $M$ is a random variable (r.v.) whose optimized Probability Density Functions (PDFs) have been determined in [23]. Beside the packet encoding in segments, in NOMA, NOMA/CRDSA, and NOMA/IRSA schemes, each user can select, among $L$ possible equally likely energy levels, that adopted for the transmission of its segments. The other schemes, i.e., SA, CRDSA, and IRSA, of course adopt $L = 1$.

At the destination, according to the IC mechanism, the segments, possibly collided but referred to already successfully decoded packets, are cancelled from the corresponding slots, thus enabling further packet decodings. To realistically account for the nonideality of IC, define as $\epsilon$ ($0 \leq \epsilon \leq 1$) the fraction of the residual interference after each cancellation cycle and consider the presence of a specific header in each segment. This header, whose effect on the final performance of each scheme will be specifically addressed in Section IV.D, contains specific pointers to the positions in the RAF of the other segments referred to the same packet. This enables the destination to infer the slots in which IC must

be performed. For such system, the instantaneous channel load can be expressed (in packets per slot) as [15]:

$$G = \chi \frac{H}{K}, \tag{1}$$

where $0 \leq \chi \leq 1$ is the activation probability. All users are assumed to adopt the same bi-dimensional modulation of order $\varsigma$ and the same code rate $\varrho$. To jointly account for these two quantities, one may usefully consider the rate [32]:

$$R = \varrho \log_2 \varsigma, \tag{2}$$

which identifies the number of information bits carried by each transmission, channel use or symbol. For the communication channel, three propagation environments are considered: a fading-less one, suitable to investigate the performance of each scheme in a not mobile scenario, and two characterized by Rayleigh fading. These ones may be slow, if the fading level in a RAF remains constant for all segments of a packet, or fast, if, instead, the segments experience different fading levels in the same RAF.

According to the above introduced scenario, the following of this section presents the technique conceived to design the energy levels of a generic NOMA/PR scheme. The here developed approach generalizes those in [38], [39], which may be viewed as special cases of the here proposed one.

### A. NOMA/PR UNDER PERFECT IC

The design of the energy levels may be suitably addressed by moving from the Shannon bound to relate the rate $R$ to the minimum SINR $\alpha$ required to correctly receive a packet. In fact, by inverting the Shannon formula, one can immediately obtain:

$$\alpha = 2^R - 1. \tag{3}$$

Define now as $E_l/N_0$ the energy $E_l$ used by the $l$-th ($l = 1, \ldots, L$) NOMA level normalized to the noise spectral density $N_0$. Let us assume $R \geq 1$ so that, for a given energy level, only one successful packet reception is allowed. According to these definitions, the normalized average Signal to Noise Ratio (SNR) can be determined as:

$$\Gamma = \frac{E_{\text{av}}/N_0}{\text{E}[M]}, \tag{4}$$

where $E_{\text{av}}/N_0$ denotes the normalized average energy and E[$M$] represents the average number of repetitions. Recalling the fundamental NOMA concept under perfect IC, the correct detection of a packet when all transmitters use different energy levels requires that the following constraint be met [6]:

$$\frac{E_l/N_0}{1 + \sum_{i=1}^{l-1} E_i/N_0} \geq \alpha, \quad l = 1, \ldots, L. \tag{5}$$

It may be shown that (5) is satisfied when the $l$-th normalized energy level is given by:

$$E_l/N_0 = \alpha_1 (1 + \alpha_1)^{l-1}, \quad l = 1, \ldots, L, \tag{6}$$

**TABLE 1.** NOMA/IRSA: Probability of selecting $M$ segments as a function of the number $L$ of energy levels.

| $L$ | $M$ | | | |
|---|---|---|---|---|
| | 2 | 3 | 4 | 8 |
| 1 | 0.5112 | 0.2660 | | 0.2228 |
| 2 | 0.6607 | 0.1605 | | 0.1788 |
| 3 | 0.7439 | 0.0906 | 0.0156 | 0.1499 |
| 4 | 0.7947 | 0.0470 | | 0.1583 |
| 5 | 0.8370 | | | 0.1630 |

**TABLE 2.** $E_{\text{av}}/N_0$ thresholds for $R = 1$ information bits/symbol.

| | NOMA | | NOMA/CRDSA | | NOMA/IRSA | |
|---|---|---|---|---|---|---|
| $L$ | $M$ | $E_{\text{av}}/N_0$ [dB] | $M$ | $E_{\text{av}}/N_0$ [dB] | E[$M$] | $E_{\text{av}}/N_0$ [dB] |
| 1 | 1 | 0.00 | 2 | 3.01 | 3.60 | 5.57 |
| 2 | 1 | 1.76 | 2 | 4.77 | 3.23 | 6.86 |
| 3 | 1 | 3.68 | 2 | 6.69 | 3.02 | 8.48 |
| 4 | 1 | 5.74 | 2 | 8.75 | 3.00 | 10.51 |
| 5 | 1 | 7.92 | 2 | 10.93 | 2.98 | 12.66 |

where $\alpha_1 = m_f \alpha$ accounts for a possible margin $m_f$. More precisely, (5) identifies, for the generic $l$-th normalized energy level, the condition to meet for ensuring the correct reception of a packet using that level, when, for all the other packets, lower and different levels are adopted. By using (6), the condition (5) is satisfied when $m_f \geq 1$. Furthermore, $m_f$ may be used to obtain a specific $\Gamma$ value given $L$. Actually, given the equal probability assumption, the normalized average energy can be expressed as:

$$\Gamma = \frac{E_{\text{av}}/N_0}{\text{E}[M]} = \frac{(1 + \alpha_1)^L - 1}{L} \geq \frac{(1 + \alpha)^L - 1}{L}. \tag{7}$$

As a possible example, Table 1 reports the probabilities, derived according to [23, Table 1], of selecting $M$ segments as a function of the number of energy levels. Using these values and fixing $L$, E[$M$], and $E_{\text{av}}/N_0$, the minimum normalized average energies (i.e., the SINR thresholds) required for the correct reception of a segment can be obtained using (7). Table 2 summarizes some values for $R = 1$, which, from (3), implies $\alpha = 1$.

### B. NOMA/PR UNDER IMPERFECT IC

Consider now the imperfect IC condition with a residual interference $\epsilon$. In the presence of this residual, the normalized energy levels become [39]:

$$\frac{E_l}{N_0} = \frac{E_L}{N_0} \beta^{L-l}, \quad l = 1, \ldots, L, \tag{8}$$

where:

$$\beta = \frac{1 + \alpha_1 \epsilon}{1 + \alpha_1}, \tag{9}$$

and:

$$\frac{E_L}{N_0} = \frac{\alpha_1 (1 - \epsilon)}{1 - \epsilon - (1 + \alpha_1 \epsilon)\left(1 - \beta^{L-1}\right)}. \tag{10}$$

In the sequel of this article, the energy levels defined by (8) with $\epsilon > 0$ will be referred to as *robust* design, while the levels obtained by (6) with $\epsilon = 0$ will be referred to as *basic* design. More precisely, by adopting a value $\epsilon > 0$ in the energy design (*robust* design), a packet using the $l$-th level is

correctly received when all the other packets use lower and different energy levels, and when the residual interference amount after IC does not exceed $\epsilon$. When $\epsilon = 0$ instead (*basic* design), perfect IC is required. The usage of the term 'robust' hence arises from the objective of making the system capable to correctly receive a packet when, realistically, a residual interference is present, a situation in which the basic design, relying on an ideal IC, would instead experience a poor performance. By recalling (4) and using (8)-(10), the normalized SNR can be expressed as:

$$\Gamma = \frac{1}{L}\frac{1-\beta^L}{\beta^L-\epsilon}, \tag{11}$$

which enables to reformulate the definition of $\beta$ in (9) when $\epsilon$, $L$, and the values of $\Gamma$ given by (4) are assigned. Accordingly, by inverting (11), one obtains:

$$\beta = \left(\frac{1+\epsilon L\Gamma}{1+L\Gamma}\right)^{1/L}, \tag{12}$$

and then, by further inverting (9), one can derive:

$$\alpha_1 = \frac{1-\beta}{\beta-\epsilon}. \tag{13}$$

Now that the NOMA levels in the presence of IC are available, it is worth to investigate their implications on the rate. In particular, $R$ must meet the following condition:

$$R < \log_2(1+\alpha_1) = \log_2\left(\frac{1-\epsilon}{\beta-\epsilon}\right), \tag{14}$$

which, for $\Gamma \to \infty$, becomes:

$$R < \log_2\left(\frac{1-\epsilon}{\epsilon^{1/L}-\epsilon}\right), \tag{15}$$

by using (12). This latter expression is interesting because it enables to derive an upper bound on the number of energy levels as:

$$L < \frac{\log\epsilon}{\log\left[2^{-R}(1-\epsilon)+\epsilon\right]}. \tag{16}$$

As possible examples, Table 3 reports the maximum number of energy levels as a function of $R$ and $\epsilon$. As expected, the number of levels, which holds both for pure NOMA and joint NOMA/PR algorithms, decreases with the increase of $\epsilon$.

**TABLE 3.** Number of energy levels $L$ as a function of the rate $R$ and of the residual interference $\epsilon$.

| $\epsilon$[%] | $R$ | | | |
|---|---|---|---|---|
| | 1 | 1.25 | 1.5 | 1.75 |
| 1 | 6 | 5 | 4 | 3 |
| 2 | 5 | 4 | 3 | 3 |
| 3 | 5 | 4 | 3 | 3 |
| 4 | 4 | 3 | 3 | 2 |
| 5 | 4 | 3 | 3 | 2 |

## III. ANALYSIS

This section presents a theoretical analysis for evaluating the success probability $P_s$ when the energy levels are defined according to (8). The derivation of $P_s$ is relevant since it enables to directly obtain the throughput $S$, which is measured as the number of information bits per transmission that are correctly decoded at the receiver. This latter quantity can be expressed as a function of the offered load $G$, of the rate $R$, and of the success probability $P_s$ as [29]:

$$S = G\,P_s\,R. \tag{17}$$

Observe that $G\,P_s$ represents the number of packets successfully received in a slot, thus it identifies the multiplexing capability of the access scheme, while the rate $R$ takes into account the transmission mode, i.e., the modulation/code pair. In (17), the key quantity for obtaining a proper throughput estimation is the success probability. Its theoretical analysis is analytically tractable when $R > 1$ and $m_f \cong 1$ in two cases: for a pure NOMA scheme in a fading-less environment, but accounting for any traffic load, and for a general NOMA/PR scheme in low traffic conditions ($G << 1$), but accounting for the presence of Rayleigh fading. These two cases are respectively analyzed in the following subsections.

### A. NOMA PERFORMANCE IN FADING-LESS SCENARIO

According to the proposed model, there are two kinds of successful events in a fading-less situation. To clarify them, assume to observe the result of the receptions from the point of view of a specific user that is attempting to send a packet (target user). The first kind of events, in which all users experience a successful decoding, involves $h = k+1 \le L$ users (the target one and the other $k$ concurrent ones), all choosing different energy levels. The second kind of events is still referred to $h = k+1$ users, but is just partly successful, since it includes some energy levels selected by more users, which leads, given the assumption $R \ge 1$, to collisions, and some other levels, selected by just one user, which may be successful. Identify by $s$ the highest collision level. In such a situation, some receptions may be successful only if there is at least one idle energy level in a position $t$ satisfying the inequality $1 \le s < t \le L$. More precisely, the $k+1$ transmitted segments may be subdivided into four groups (Fig. 1): the $n_s$ successful ones ($1 \le n_s \le L-t = n_p$), the $n_u = t-s-1$ unsuccessful ones that individually select an energy level between $s$ and $t$, the $n_c \ge 2$ ones that collide in the $s$-th level, and the $n_f = h - n_s - n_u - n_c$ ones that select an energy level between 1 and $s-1$ when $s > 1$. Following this classification, the success probability given $k$

$$P_{s|k} = \frac{1}{L^{k+1}}\left[\sum_{n_c=2}^{k}\sum_{s=2}^{L-2}\sum_{t=s+1}^{t_{\max}}\sum_{n_s=1}^{n_{s\max}}\frac{k!}{n_c!}\binom{n_p}{n_s}n_s\frac{(s-1)^{n_f}}{n_f!} + \sum_{n_c=n_{c\min}}^{k}\sum_{t=2}^{t_{\max 2}}\frac{k!}{n_c!}\binom{n_p}{n_s}n_s + u(L-k)\frac{L!}{(L-k-1)!}\right] \tag{18}$$

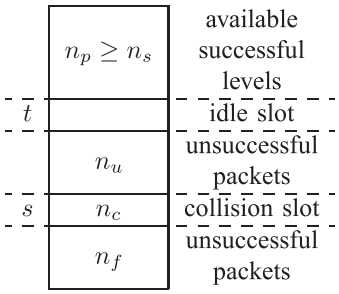


**FIGURE 1.** Collision model.

**TABLE 4.** Closed-form NOMA success probabilities for the first four $L$ values.

| $L$ | $P_s$ |
|---|---|
| 1 | $e^{-G}$ |
| 2 | $e^{-G}\left(1+\frac{G}{2}\right)$ |
| 3 | $\frac{e^{-G}}{9}\left(6+5G+G^2+3e^{G/3}\right)$ |
| 4 | $\frac{e^{-G}}{64}\left[32+28G+9G^2+G^3+16e^{G/2}+8(2+G)e^{G/4}\right]$ |

can be evaluated according to (18), reported at the bottom of the previous page, where:

$$t_{\max} = \min(L-1, h-n_c+s), \tag{19a}$$

$$n_{s\max} = \min\big(n_p, h-n_c-n_u\big), \tag{19b}$$

$$n_{c\min} = \max(2, h-L+2), \tag{19c}$$

$$t_{\max_2} = \min(L-1, 1+h-n_c), \tag{19d}$$

and $u(x)$ denotes the unit step function ($u(x)=1$ if $x>0$, $u(x)=0$ otherwise). In (18), the first addendum corresponds to the collision scenario when $s>1$, the second addendum models the collision scenario when $s=1$, while the third addendum corresponds to the fully successful scenario. Assuming a Poisson traffic, from (18) it is possible to determine the average successful probability as:

$$P_s = \sum_{k=0}^{\infty} P_{s|k}\frac{G^k}{k!}\exp(-G). \tag{20}$$

This latter formula may be evaluated in closed-form for different $L$ values. Some expressions are reported in Table 4. Observe that, for $L=1$, we obtain the well known success probability for the SA protocol.

### *B. NOMA/PR LIMITING PERFORMANCE IN FADING SCENARIO*

At very low traffic, the collision is an unlikely event. This simplifies the analysis developed in the previous subsection and enables to include fading effects in the general NOMA/PR scenario. Observe that, from the point of view of the success probability, fading may reduce the received signal level below the decoding threshold, but may also have a positive effect in case of collision, since it may reduce the interference level due to some segments. In low load conditions, this positive effect is however negligible. For this reason, the estimators presented below are considered approximating upper bounds.

When the fading statistic is introduced in the analysis, the normalized SNR defined by (4) may be viewed as its average value. Hence, assuming a Rayleigh fading channel, the actual SNR $\gamma$ is described by an exponential r.v., whose Cumulative Distribution Function (CDF) is given by:

$$F(\gamma,\Gamma) = \big[1-\exp(-\gamma/\Gamma)\big]\mathbb{1}_{\mathbb{R}_0^+}(\gamma), \tag{21}$$

where $\mathbb{R}_0^+$ is the set of nonnegative real numbers, and $\mathbb{1}_{\mathbf{X}}(x)$ is the indicator function, that is, $\mathbb{1}_{\mathbf{X}}(x)=1$ if $x\in\mathbf{X}$ and $\mathbb{1}_{\mathbf{X}}(x)=0$ if $x\notin\mathbf{X}$. For a NOMA/PR system, it is useful to consider, for comparison purposes, both the commonly adopted single-slot model and the more advanced multi-slot one, which enables to apply Chase combining or, if incremental redundancy is used, joint decoding. Besides, it is interesting to consider slow and fast fading conditions, and also the possibility to transmit the segments with independent or identical energy levels. The complete analysis of all these possibilities leads to four different upper bounds for the success probability of each decoding model (single-slot, multi-slot with Chase combining, multi-slot with joint decoding). Observe that, for the PR schemes in single-slot scenario, it is sufficient to consider only the best segment. In an equal energy scenario with slow fading, all the segments experience the same conditions, while in independent energy scenarios and/or in the presence of fast fading, a transmission attempt fails only when all the segments fail. In the Chase and code combining scenarios, instead, all the segments should be considered. The following paragraphs explain these aspects in more detail by presenting the success probability upper bounds for each receiving model.

#### 1) SINGLE-SLOT DETECTION

As a first step, it is useful to define the probability $p_l$ that the fading level exceeds the threshold of correct reception for the $l$-th energy level without exceeding the threshold of the $(l+1)$-th one. This probability is given by:

$$p_l = F\left(\alpha, \frac{E_l}{N_0}\right) - F\left(\alpha, \frac{E_{l+1}}{N_0}\right), \quad l=1\cdots L, \tag{22}$$

where the term $E_{L+1}/N_0=\infty$ is introduced for mathematical purposes. Assuming a slow fading scenario, the probability of a single attempt failure when the fading level lies between the $l$-th and the $(l+1)$-th energy levels is given by $p_{f|l}=l/L$. Considering a constant level for the $M$ segments, $l/L$ represents also the failure probability for all of them. Thus, the success probability is upper bounded by:

$$P_s \leq 1-\sum_{l=1}^{L} p_l\frac{l}{L}. \tag{23}$$

If, instead, independent levels are considered, the reception fails if all the $M$ segments fail. Given the energy level, this event occurs with probability $(l/L)^m$. Therefore, the success probability becomes upper bounded by:

$$P_s \leq 1 - \sum_{l=1}^{L} p_l \sum_{m=1}^{M} \left(\frac{l}{L}\right)^m P(m), \tag{24}$$

where $P(m)$ is the probability of generating $m$ segments per packet. More precisely, for CRDSA, in which $M = 2$, we have $P(1) = 0$ and $P(2) = 1$, while, for IRSA, in which $M$ is a r.v., the corresponding probabilities are those reported in Table 1.

For a fast fading scenario, it is useful to preliminarily define the probability:

$$q_l = F\left(\alpha, \frac{E_l}{N_0}\right), \tag{25}$$

that the attempt using the $l$-th level fails. When equal energy levels are used, the success probability is upper bounded by:

$$P_s \leq 1 - \frac{1}{L} \sum_{m=1}^{M} P(m) \sum_{l=1}^{L} q_l^m. \tag{26}$$

When, instead, independent levels are used, the upper bound becomes:

$$P_s \leq 1 - \sum_{m=1}^{M} P(m) p_{f_1}^m, \tag{27}$$

where:

$$p_{f_1} = \frac{1}{L} \sum_{l=1}^{L} q_l, \tag{28}$$

represents the probability that a single attempt fails.

### 2) MULTI-SLOT DETECTION WITH CHASE COMBINING

When multi-slot detection is applied, the decision jointly involves all segments. This is significantly different from the previously analyzed single-slot case, where the decision was based on the best segment, i.e., that with the highest SINR. In particular, adopting a capture-based reception criterion in combination with Chase combining, the performance depends on the sum of the SINR values of the $M$ segments.

Let's again start with the slow fading scenario. If a transmitter uses $m$ independent energy levels $\mathbf{l}_m = [l_1, l_2, \ldots, l_m]$ for its segments, one can determine the corresponding failure probability as:

$$P_f(\mathbf{l}_m) = F\left(\alpha, \frac{1}{N_0} \sum_{l \in \mathbf{l}_m} E_l\right). \tag{29}$$

According to this definition, the upper bound for the success probability can be expressed as:

$$P_s \leq 1 - \sum_{m=1}^{M} \frac{P(m)}{L^m} \sum_{\mathbf{l}_m} P_f(\mathbf{l}_m). \tag{30}$$

If, instead, the transmitter uses the same energy level for the $m$ segments, the success probability is upper bounded by:

$$P_s \leq 1 - \frac{1}{L} \sum_{m=1}^{M} P(m) \sum_{l=1}^{L} F\left(\frac{\alpha}{m}, \frac{E_l}{N_0}\right). \tag{31}$$

For the fast fading scenario with equal energy levels, let's preliminarily define the CDF of the sum of $m$ exponential r.v.s with equal average value $\Xi$ as:

$$Q(\xi, \Xi, m) = \left[1 - \exp\left(-\frac{\xi}{\Xi}\right) \sum_{k=0}^{m-1} \frac{1}{k!} \left(\frac{\xi}{\Xi}\right)^k\right] \mathbb{1}_{\mathbb{R}_0^+}(\xi), \tag{32}$$

which represents the Erlang distribution. Exploiting this definition, the upper bound on the success probability can be evaluated as:

$$P_s \leq 1 - \frac{1}{L} \sum_{m=1}^{M} P(m) \sum_{l=1}^{L} Q\left(\alpha, \frac{E_l}{N_0}, m\right). \tag{33}$$

If, instead, the users adopt independent energy levels, it is necessary to first consider the vector $\Xi_m = [\Xi_1, \ldots, \Xi_m]$ of the possible different average values and then evaluate the CDF:

$$\mathbf{Q}(\xi, \Xi_m, m) = \left[1 - \sum_{k=1}^{m} \exp\left(-\frac{\xi}{\Xi_k}\right) \frac{\Xi_k^{m-1}}{\prod_{h \neq k}(\Xi_k - \Xi_h)}\right] \times \mathbb{1}_{\mathbb{R}_0^+}(\xi), \tag{34}$$

which holds for $\Xi_1 \neq \Xi_2 \neq \cdots \neq \Xi_m$, but allows the evaluation of all the other combinations through the extension by continuity of (34). The upper bound for the success probability can now be evaluated by taking into account all the combinations $\mathbf{E}_{\mathbf{l}m}$ of energy values as:

$$P_s \leq 1 - \sum_{m=1}^{M} \frac{P(m)}{L^m} \sum_{\mathbf{E}_{\mathbf{l}_m}} \mathbf{Q}\left(\alpha, \frac{\mathbf{E}_{\mathbf{l}m}}{N_0}, m\right). \tag{35}$$

### 3) MULTI-SLOT DETECTION WITH JOINT DECODING

For code combining, the performance depends on the sum of the equivalent rates of the individual segments. The concept of equivalent rate has been defined and deeply discussed in [32]. It substantially represents the average value of the rates of the segments associated to a packet and depends on the fading statistic. More precisely, in a slow Rayleigh fading scenario when the Shannon bound is adopted, the CDF of the equivalent rate $r$ is given by [32]:

$$T(r, \Gamma) = F\left(2^r - 1, \Gamma\right). \tag{36}$$

If the transmitters use independent energy levels, we can then identify the vector of the equivalent rates as:

$$\mathbf{R}_m = \log_2\left(1 + \frac{\mathbf{E}_{\mathbf{l}m}}{N_0}\right). \tag{37}$$

Exploiting these definitions, the upper bound of the success probability may be evaluated as:

$$P_s \leq 1 - \frac{1}{L^m} \sum_{m=1}^{M} P(m) \sum_{\mathbf{R}_m} P_f(\mathbf{R}_m), \tag{38}$$

**TABLE 5. Parameter values.**

| Parameter | Value |
|---|---|
| $E_{\text{av}}/N_0$ [dB] | 16 |
| $K$ [slots] | 20 |
| $\epsilon$ [%] | $\leq 5$ |
| $R$ [information bits/transmission] | 1 |

where $P_f(\mathbf{R}_m)$ denotes the failure probability as a function of the rate vector. For this latter quantity, a general formula holding for any $M$ value is difficult to derive. However, a closed-form expression may be calculated for the relevant $M = 2$ case as:

$$P_f(\mathbf{R}_m) = P_f(R_1, R_2) = 1 - \exp\left(\frac{\sqrt{\xi^2 + 4\delta\alpha} - \xi}{2\delta}\right), \quad (39)$$

in which $\xi = (E_{l_1} + E_{l_2})/N_0$ and $\delta = E_{l_1}E_{l_2}/N_0^2$. When the transmitters use the same energy level, instead, the upper bound of the success probability may be more simply evaluated by recalling (36), so as to obtain:

$$P_s \leq 1 - \frac{1}{L}\sum_{m=1}^{M} P(m) \sum_{l=1}^{L} T\left(\frac{R}{m}, \frac{E_l}{N_0}\right). \quad (40)$$

For the fast fading scenario, the CDF of the sum of the equivalent rates corresponding to $m$ segments is too complex and has to be determined by numerical techniques. This implies that also the corresponding bounds for the success probability with independent and equal energy levels must be numerically estimated.

## IV. RESULTS

The default parameters adopted to derive the results are reported in Table 5. These values have been chosen because they represent sensible scenarios, with limited energy, limited delay, and realistic IC factors. In particular, the unity rate $R$ is the limiting value for the NOMA throughput estimation developed in Section III.A. The impact of each parameter on the network performance has been investigated by moving from the initial values in the table. In all the evaluations, $L$ has been selected as the highest integer complying with (7). Besides, according to the system model in Section II, the input traffic is generated according to a Poisson process. Both the theoretical analysis and the simulations are implemented in MATLAB. In particular, each point of a simulated curve is obtained through Monte Carlo simulations by averaging the results derived over 1000 realizations.

### A. BOUND VALIDATION

The first group of results aims to prove the correctness of the analysis by comparing the theoretical upper bounds on the success probability calculated in Section III.B with the corresponding $P_s$ values obtained through simulations. Table 6 reports the results of this comparison for NOMA/CRDSA ($M = 2$) using the basic design. One may immediately notice that each bound is very tight to the corresponding actual

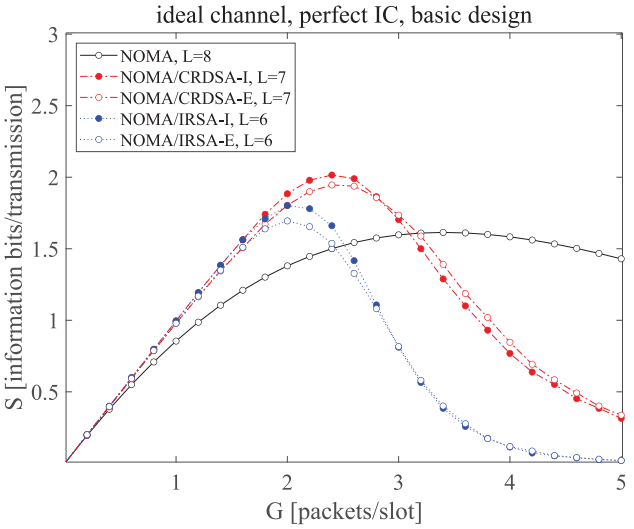


**FIGURE 2. Throughput as a function of the channel load in a fading-less scenario with perfect IC.**

success probability. This confirms the acceptability of the adopted approximation, holding in low traffic conditions, which consists in the negligibility of the positive effects of fading to possibly increase the received power for a segment. Some case by case comparisons may be also useful to put into evidence some general aspects. In particular, given the decoding model and the energy policy, fast fading always leads to larger $P_s$ values with respect to slow fading, since, in the first case, the propagation channel introduces a higher diversity. For similar reasons, given the fading scenario and the decoding model, the adoption of independent energy levels is preferable to the usage of equal ones. Finally, as expected, when the fading scenario and the energy policy are fixed, the more sophisticated the decoding model the higher the success probability. The same agreement between theory and simulations has been observed for the NOMA/IRSA scheme and for the robust design.

### B. SINGLE-SLOT MODEL

Consider now the throughput achievable by the different schemes. To this aim, let's initially focus on the basic design in a fading-less scenario with perfect IC. Figs. 2 and 3 illustrate the throughput and the success probability, respectively, for pure NOMA and NOMA/PR schemes, where the termination '-I' identifies the usage of independent energy levels (also identified by filled markers), while the termination '-E' identifies the usage of equal energy levels (also identified by empty markers). The first of these two figures shows that joint NOMA/CRDSA has a slightly better performance at low loads, while pure NOMA is better at high loads. Joint NOMA/IRSA has a slightly worse performance, given the limited energy and the low number of slots available in the RAF. For both joint PR schemes, the independent energy design parallels the equal energy one. Fig. 3 puts instead into evidence the most important benefit of the repetition schemes with respect to pure NOMA: the capability to

**TABLE 6.** Theoretical upper bounds and simulated success probabilities for NOMA/CRDSA with $L = 7$ using the basic design ($\epsilon = 0$) and considering different fading scenarios, decoding criteria, and energy level selection policies.

| Decoding model | Fading scenario | Energy levels | Theory | Simulation | Confidence interval |
|---|---|---|---|---|---|
| single-slot | slow | equal | 0.797 | 0.793 | 7.01E-03 |
| single-slot | slow | independent | 0.906 | 0.906 | 2.96E-03 |
| single-slot | fast | equal | 0.915 | 0.918 | 3.82E-03 |
| single-slot | fast | independent | 0.959 | 0.960 | 5.21E-03 |
| multi-slot with Chase combining | slow | equal | 0.883 | 0.885 | 4.74E-03 |
| multi-slot with Chase combining | slow | independent | 0.933 | 0.933 | 3.59E-03 |
| multi-slot with Chase combining | fast | equal | 0.947 | 0.946 | 4.29E-03 |
| multi-slot with Chase combining | fast | independent | 0.975 | 0.975 | 1.13E-03 |
| multi-slot with code combining | slow | equal | 0.901 | 0.901 | 6.45E-03 |
| multi-slot with code combining | slow | independent | 0.941 | 0.942 | 2.62E-03 |
| multi-slot with code combining | fast | equal | 0.957 | 0.957 | 3.97E-03 |
| multi-slot with code combining | fast | independent | 0.980 | 0.980 | 5.29E-04 |

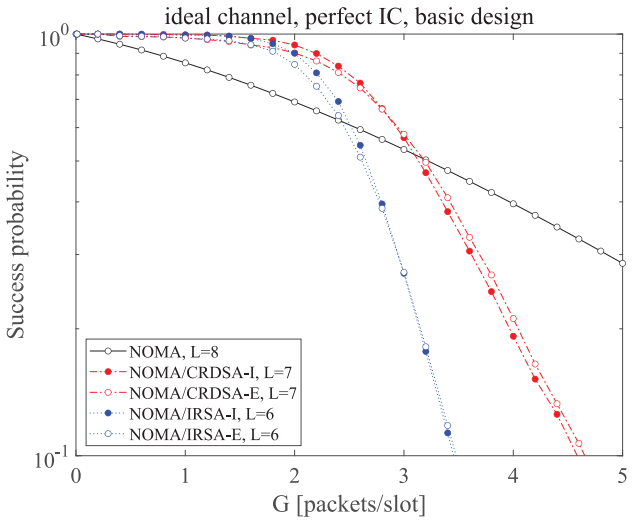


**FIGURE 3.** Success probability as a function of the channel load in a fading-less scenario with perfect IC.

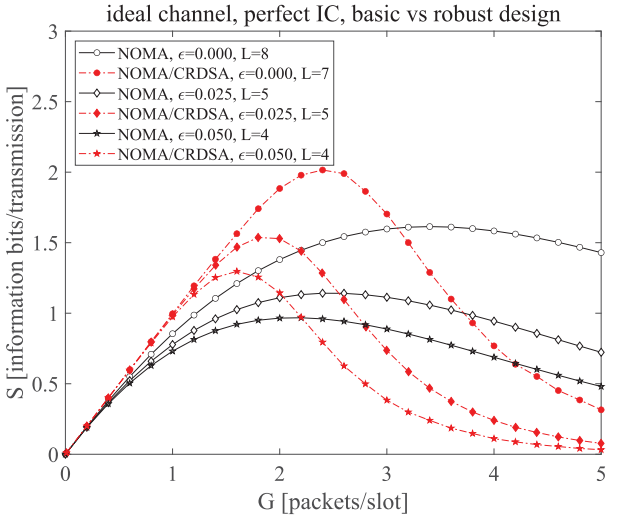


**FIGURE 4.** Throughput as a function of the channel load in a fading-less scenario using a robust design.

almost completely deliver the packets from low to moderate loads. This represents a general, basic difference between pure NOMA and both pure and joint PR-based techniques, which will remain observable for all the situations addressed in the remaining of this article.

Consider now the robust design, which has been specifically conceived to operate in the presence of a residual interference $\epsilon$. Note that this characteristic does not imply its sole usage under imperfect IC. It might be in fact even used with perfect IC, but at the expense of a certain performance reduction. To this aim, Fig. 4 quantifies the throughput deriving from adopting the robust design in NOMA and NOMA/CRDSA for different $\epsilon$ values. This figure highlights the impact of this latter parameter on the performance, whose reduction with the increase of $\epsilon$ is significant.

The subsequent group of results in Fig. 5 outlines the impact of fading by showing the throughput for the slow fading case when the basic design is adopted. The curves confirm that the independent energy design outperforms the fixed energy one, a result already observed in Table 6 from the analysis of the theoretical and numerical upper bounds. A comparison, still in a slow fading scenario, between the basic ($\epsilon = 0$) and the robust ($\epsilon = 0.05$) designs is reported in Fig. 6. This figure reveals that, in realistic conditions, the performance of the robust design parallels that of the basic one in terms of maximum throughput. One may however specifically note that, in low traffic conditions, the robust design is preferable to the basic one, while, for higher loads, the opposite choice should be carried out. The better performance of the robust design for low traffic loads is confirmed by Table 7, which focuses on the success probability by considering the simulated values and the theoretical upper bounds in both slow and fast fading scenarios. In particular, the values in this table extend to the fast fading scenario the observations so far formulated on the suitability of the robust design in low traffic conditions.

As a summary of the results obtained for the single-slot model, one may notice that the major advantage of the joint NOMA/PR techniques is their higher success probability at low to moderate loads (Fig. 3). In fact, $P_s$ approaches 1 in fading-less conditions and remains satisfactorily close to this value in different fading scenarios (Table 6). Joint NOMA/PR

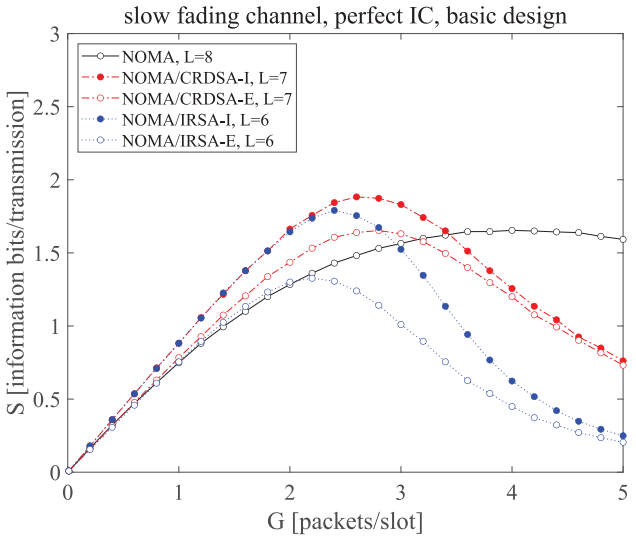


**FIGURE 5.** Throughput as a function of the channel load in slow fading scenario with perfect IC using a basic design.

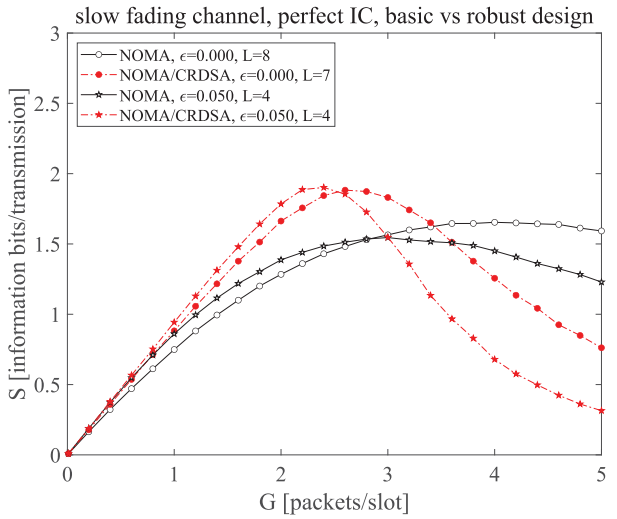


**FIGURE 6.** Throughput as a function of the channel load in slow fading scenario with perfect IC. Comparison between basic and robust designs.

**TABLE 7.** Theoretical upper bounds and simulated success probabilities for NOMA/CRDSA obtained with independent energy levels using the single-slot decoding model in the presence of different fading scenarios and designs.

| Design | $\epsilon$ | L | Fading scenario | Theory | Simulation | Confidence interval |
|---|---|---|---|---|---|---|
| basic | 0.00 | 7 | slow | 0.906 | 0.906 | 2.96E-03 |
| robust | 0.05 | 4 | slow | 0.948 | 0.948 | 5.86E-03 |
| basic | 0.00 | 7 | fast | 0.959 | 0.960 | 5.21E-03 |
| robust | 0.05 | 4 | fast | 0.993 | 0.993 | 3.46E-03 |

techniques have also a slightly higher maximum throughput, and the advantage is significant at low loads, while pure NOMA has a higher throughput at high loads. In ideal conditions, the not necessary usage of the robust design may cause a reduction of the throughput, but, in realistic conditions, it allows a higher success probability, being able to sustain a given degree of imperfect IC.

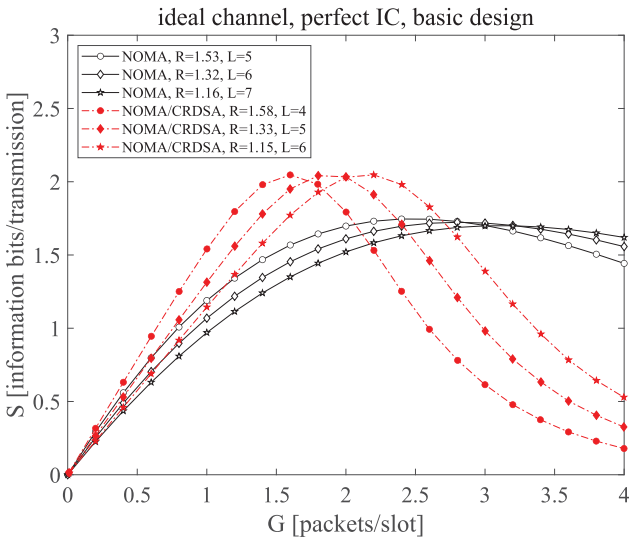


**FIGURE 7.** Throughput for different rates $R$ in ideal conditions with perfect IC.

### C. IMPACT OF THE PARAMETERS

This section investigates in more detail the effects of the parameters on the performance. To this purpose, consider first the rate $R$. This quantity must meet the condition (14), which depends on the access technique and on its parameters $L$, $M$, $\epsilon$, $E_{\text{av}}/N_0$. Besides, by (17), the throughput directly depends on $R$. To this regard, note that, in this article, the condition $R \geq 1$ has been always assumed in order to exclude the situations in which more than one packet is successfully detected in a collision. To discuss the effects of $R$ on the performance, initially consider the access techniques with a single energy level ($L = 1$), such as pure SA ($M = 1$) and CRDSA ($M = 2$) for $E_{\text{av}}/N_0 = 16$ dB (Table 5). In such cases, $R$ must meet the condition $R < \log_2(1 + \Gamma)$, which leads, for SA, to $R < 5.35$ and $S \approx 5.35/e \approx 1.97$ (both given in information bits/transmission). For CRDSA, instead, one obtains, still in information bits/transmission, $R < 4.39$ and a maximum throughput $S = 2.19$ by assuming $GP_s = 0.5$, a value that can be approached when $K \to \infty$. These values are comparable with the maximum throughput of the joint NOMA/CRDSA access technique, shown in Fig. 2. Thus, for the single-slot detection model, the performance of pure CRDSA parallels that of joint NOMA/CRDSA, although the performance of the latter may be improved by increasing $K$. A higher throughput may be obtained by using IRSA with a sufficiently large $K$ value. Furthermore, when $R$ is limited within a specific range, for example forcing the usage of a Quadrature Phase-Shift Keying (QPSK) modulation, which leads to $R \leq 2$, the performance of pure CRDSA becomes much lower. The effects of this limitation for pure NOMA and NOMA/CRDSA are addressed in Fig. 7 by considering different $L$ values and designing the $R$ ones to comply with (14) when $\epsilon = 0$. This figure shows that the maximum offered load increases with the decrease of $R$, but the maximum throughput remains almost constant. The effect

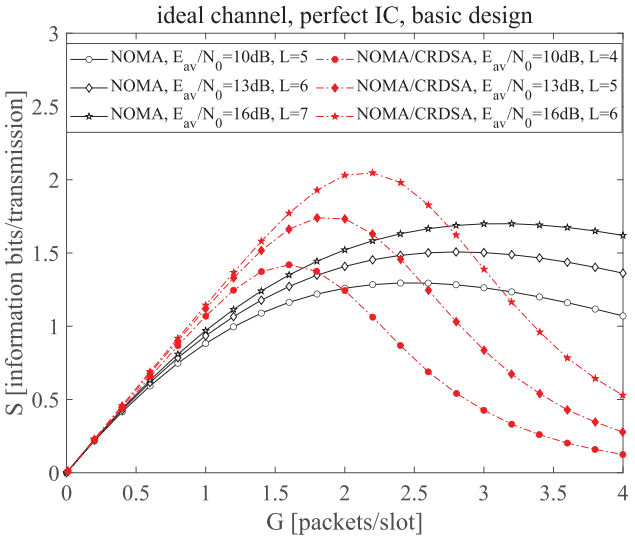


**FIGURE 8.** Throughput for different average signal to noise ratios $E_{av}/N_0$ in ideal conditions with perfect IC for $R \approx 1.15$.

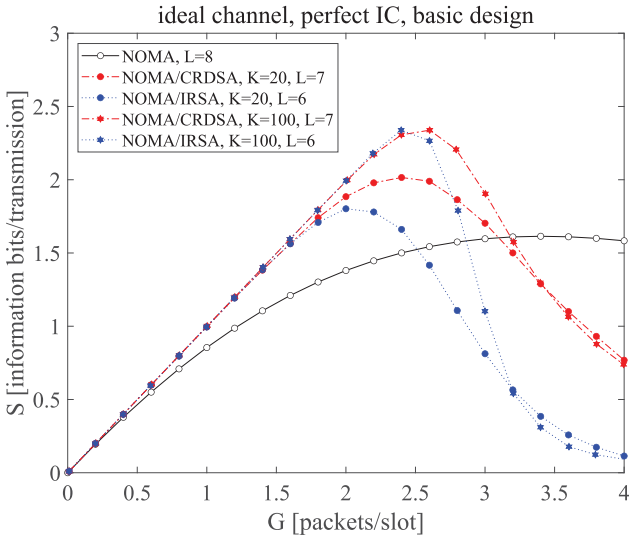


**FIGURE 9.** Throughput for different RAF lengths $K$ in ideal conditions with perfect IC.

of the reduction of $R$ is substantially that of increasing the performance of the scheme at the higher loads at the cost of a reduction at the lower ones.

Consider now the effects of the energy on the performance by analyzing Fig. 8, which is obtained for different normalized average energies $E_{av}/N_0$ when the rate is still designed according to (14) for $\epsilon = 0$. As expected, the increase of the energy and hence of the number of levels leads to a higher diversity, thus improving the performance. More precisely, the figure puts into evidence that the throughput improvement experienced by the joint NOMA/CRDSA scheme is higher than that provided by the pure NOMA one.

Finally, let's observe the impact of the RAF length on the throughput. Fig. 9 puts into evidence that both analyzed NOMA/PR schemes benefit from the increase of the number of available slots, even if the highest gain in terms of maximum throughput when the RAF length increases from $K = 20$ to $K = 100$ is obtained by the joint NOMA/IRSA scheme. Summarizing, the pure techniques, such as SA, CRDSA, and IRSA, may obtain a good performance if the modulation can be adaptively selected. In particular, CRDSA and IRSA achieve their limiting throughput by using large $K$ values, a choice that however implies large delays. Assuming instead some constraints on the choice of the modulation, joint techniques may be preferable, having the maximum throughput of NOMA/CRDSA only a weak dependence on $R$.

### D. CHASE COMBINING AND JOINT DECODING

Consider now, beside the single-slot model (maximum SINR), the more advanced multi-slot ones represented by Chase combining (sum of SINRs) and joint decoding (sum of equivalent rates) [36]. For properly exploiting the benefits of these detection techniques, the position of all the $M$ segments should be known in advance, before performing packet decoding. Therefore, a header must be enclosed in each segment to determine the positions of the other segments of the same packet. This header may have a strong impact on the throughput, especially for large $M$ values. Hence, before presenting the achievable performance, it is worth to briefly summarize the header characteristics.

When $M$ replicas are generated and the RAF consists of $K$ slots, $b = \lceil \log_2 K \rceil$ bits are required to specify the position of each segment belonging to the same packet. Therefore, the header should include at least $b(M-1)$ bits, even if header compression may be used to reduce the overhead. To enable packet reception and IC, at least one among the $M$ headers should be correctly decoded. This operation depends on the decoding strategy. For the single-slot model, the header and the packet adopt the same coding rate, being the success condition identical for them. For the multi-slot decoding strategies the situation differs, since at least one header must be correctly received before performing packet decoding. If Chase combining is adopted, the condition for correct packet decoding can be given in terms of the rate $R$ as:

$$R < \log_2\left(1 + \sum_{m=1}^{M} \gamma_m\right), \tag{41}$$

where $\gamma_m$ is the actual SINR of the $m$-th segment. Concerning the $M$ headers, the one with the best SINR is characterized by $\gamma_h = \max_m(\gamma_m)$. Hence, from (41), we can infer the following requirement:

$$\gamma_h \geq \frac{1}{M} \sum_{m=1}^{M} \gamma_m, \tag{42}$$

which, in turn, leads to the following constraint for the corresponding header rate:

$$R_h \leq \log_2\left(1 + \frac{2^R - 1}{M}\right). \tag{43}$$

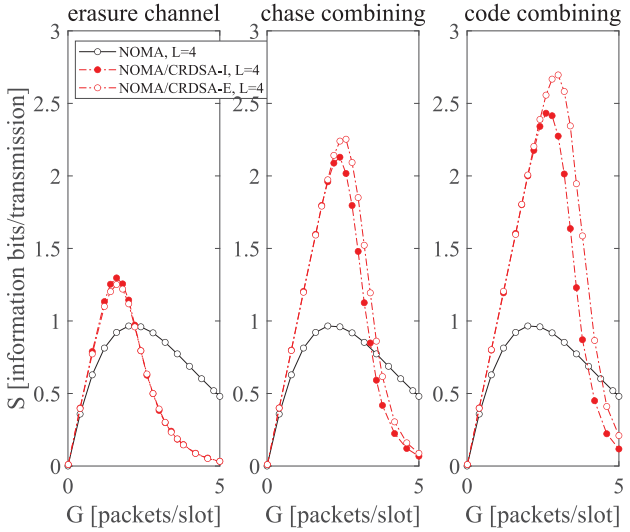


**FIGURE 10.** Throughput as a function of the channel load in ideal conditions and perfect IC assuming a robust design.

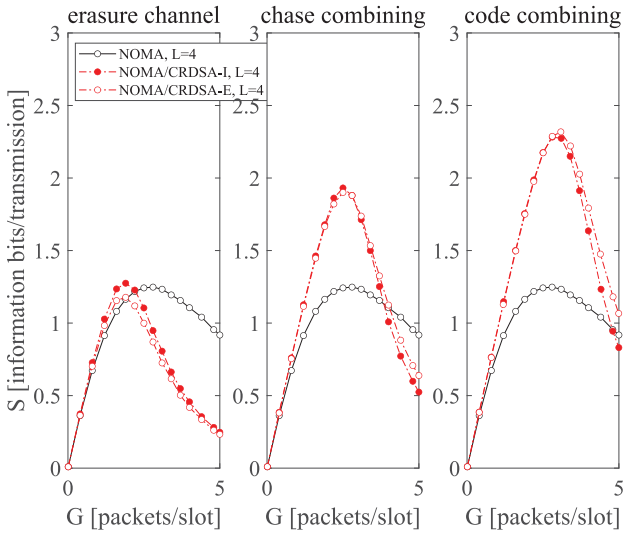


**FIGURE 11.** Throughput as a function of the channel load in a slow fading scenario with imperfect IC assuming a robust design.

If, instead, code combining is used, the header rate must satisfy this other constraint:

$$R_h \leq \frac{R}{M}. \tag{44}$$

The above discussion shows that the effect of the header on the performance may be determined by considering the packet information size, the number of slots per RAF, and the number of segments. More precisely, this effect is heavy on NOMA/IRSA (large $M$ values) and less significant for NOMA/CRDSA ($M = 2$). For this reason and for its wider usage in current satellite systems [17], the results presented in this section are focused on NOMA/CRDSA. In particular, Fig. 10 compares the performance of the three different decoding techniques in ideal conditions for the robust design. As expected, the more sophisticated the reception criterion, the higher the throughput for the NOMA/CRDSA scheme with independent and equal energy levels from low to moderate loads. Conversely, pure NOMA, being characterized by the transmission of a unique packet copy, is not capable to exploit the benefits of multi-slot decoding in the same traffic conditions, but becomes again preferable when the load gets significant. This trend is confirmed by the final figure, still derived for the robust design, but in slow fading conditions with imperfect IC (Fig. 11). In this situation, the fading has a positive effect on the NOMA performance and a slightly negative effect on the NOMA/CRDSA one. However, the advantage of the joint system remains significant for the code combining detection model. This advantage may be also improved by increasing the RAF duration. Note that, to fairly compare the three decoding techniques, the robust design has been adopted in all the evaluations of this subsection, although this specific design is mandatory only for the results presented in the last figure, which addresses the realistic situation in which a residual interference remains present after cancellation.

## V. CONCLUSION

Next generation networks will support a large amount of uncoordinated sporadic traffic coming from a large number of nodes that attempt to simultaneously communicate with a common receiver. For such kind of traffic, SA represents a suitable access technique, but, in its basic behavior, may have a not satisfactory performance. Multiple energy levels provided by NOMA may be used to obtain a first kind of diversity for improving the throughput. Besides, PR schemes (IRSA and CRDSA) may be adopted to introduce a second kind of diversity, which allows one to improve the system reliability by exploiting an increased delay and complexity.

This article has explored the joint utilization of multiple energy levels and repetition schemes to increase both the throughput and the reliability of the random access scheme. This task has been carried out by assuming suitable energy constraints and realistic operation conditions, including imperfect IC and packet overhead. The results have confirmed that one important benefit of repetition schemes is the delivery of almost all packets at low to moderate loads, while for schemes not adopting repetitions this is not the case. However, to fully exploit the repetition schemes capabilities, a large RAF duration should be used, and advanced detection schemes, such as Chase combining or joint decoding, should be adopted. To this end, a suitable, self-decodable header should be added to each segment of a packet to infer the position in the RAF of the other segments referred to the same packet. The influence of this header has been investigated for the more diffused NOMA/CRDSA scheme by showing that the introduced overhead has an acceptable impact on the throughput, specially for low $M$ values. A final and positive aspect that is worth to consider when combined NOMA/PR protocols are conceived is that the complexity derived by the joint introduction of two diversity techniques is mainly at charge of the common receiver, while

the transmitters (sensors, actuators) maintain their desired technological simplicity.

## REFERENCES


[1] A. S. Lalos, M. Di Renzo, L. Alonso, and C. Verikoukis, "Impact of correlated log-normal shadowing on two-way network coded cooperative wireless networks," *IEEE Commun. Lett.*, vol. 17, no. 9, pp. 1738–1741, Sep. 2013.

[2] A. Antonopoulos, A.S. Lalos, M. Di Renzo, and C. Verikoukis, "Cross-layer theoretical analysis of NC-aided cooperative ARQ protocols in correlated shadowed environments," *IEEE Trans. Veh. Technol.*, vol. 64, no. 9, pp. 4074–4087, Sep. 2015.

[3] M. Di Renzo, "Stochastic geometry modeling and analysis of multi-tier millimeter wave cellular networks," *IEEE Trans. Wireless Commun.*, vol. 14, no. 9, pp. 5038–5057, Sep. 2015.

[4] F. Babich and M. Comisso, "Including the angular domain in the analysis of finite multi-packet peer-to-peer networks with uniformly distributed sources," *IEEE Trans. Commun.*, vol. 64, no. 6, pp. 2494–2510, Jun. 2016.

[5] L. G. Roberts, "ALOHA packet systems with and without slots and capture," Rep. ARPANET System Note 8 (NIC11290), ARPANET Syst., Fort Meade, MD, USA, Jun. 1972.

[6] C. Xu, L. Ping, P. Wang, S. Chan, and X. Lin, "Decentralized power control for random access with successive interference cancellation," *IEEE J. Sel. Areas Commun.*, vol. 31, no. 11, pp. 2387–2395, Nov. 2013.

[7] Y. Liu, Z. Qin, M. Elkashlan, Z. Ding, A. Nallanathan, and L. Hanzo, "Nonorthogonal multiple access for 5G and beyond," *Proc. IEEE*, vol. 105, no. 12, pp. 2347–2381, Dec. 2017.

[8] Z. Ding *et al.*, "Application of non-orthogonal multiple access in LTE and 5G networks," *IEEE Commun. Mag.*, vol. 55, no. 2, pp. 185–191, Feb. 2017.

[9] S. M. R. Islam, N. Avazov, O. A. Dobre, and K. Kwak, "Power-domain non-orthogonal multiple access (NOMA) in 5G systems: Potentials and challenges," *IEEE Commun. Surveys Tuts.*, vol. 19, no. 2, pp. 721–742, 2nd Quart., 2017.

[10] L. Dai, B. Wang, Y. Yuan, S. Han, I. Chih-Lin, and Z. Wang, "Non-orthogonal multiple access for 5G: Solutions, challenges, opportunities, and future research trends," *IEEE Commun. Mag.*, vol. 53, no. 9, pp. 74–81, Sep. 2015.

[11] Z. Ding, X. Lei, G. K. Karagiannidis, R. Schober, J. Yuan, and V. K. Bhargava, "A survey on non-orthogonal multiple access for 5G networks: Research challenges and future trends," *IEEE J. Sel. Areas Commun.*, vol. 35, no. 10, pp. 2181–2195, Oct. 2017.

[12] Y. Cai, Z. Qin, F. Cui, G. Y. Li, and J. A. McCann, "Modulation and multiple access for 5G networks," *IEEE Commun. Surveys Tuts.*, vol. 20, no. 1, pp. 629–646, 1st Quart., 2018.

[13] S. M. R. Islam, M. Zeng, O. A. Dobre, and K. Kwak, "Resource allocation for downlink NOMA systems: Key techniques and open issues," *IEEE Wireless Commun.*, vol. 25, no. 2, pp. 40–47, Apr. 2018.

[14] W. Shin, M. Vaezi, B. Lee, D. J. Love, J. Lee, and H. V. Poor, "Non-orthogonal multiple access in multi-cell networks: Theory, performance, and practical challenges," *IEEE Commun. Mag.*, vol. 55, no. 10, pp. 176–183, Oct. 2017.

[15] E. Casini, R. De Gaudenzi, and O. del Rio Herrero, "Contention resolution diversity slotted ALOHA (CRDSA): An enhanced random access schemefor satellite access packet networks," *IEEE Trans. Wireless Commun.*, vol. 6, no. 4, pp. 1408–1419, Apr. 2007.

[16] G. Liva, "Graph-based analysis and optimization of contention resolution diversity slotted ALOHA," *IEEE Trans. Commun.*, vol. 59, no. 2, pp. 477–487, Feb. 2011.

[17] *Second Generation DVB Interactive. Satellite System (DVB-RCS2); Part 2: Lower Layers for Satellite Standard*, Standard ETSI EN 301 545-2 V1.2.1, 2014.

[18] L. Toni and P. Frossard, "Prioritized random MAC optimization via graph-based analysis," *IEEE Trans. Commun.*, vol. 63, no. 12, pp. 5002–5013, Dec. 2015.

[19] E. Paolini, G. Liva, and M. Chiani, "Coded slotted ALOHA: A graph-based method for uncoordinated multiple access," *IEEE Trans. Inf. Theory*, vol. 61, no. 12, pp. 6815–6832, Dec. 2015.

[20] J. Choi, "NOMA-based random access with multichannel ALOHA," *IEEE J. Sel. Areas Commun.*, vol. 35, no. 12, pp. 2736–2743, Dec. 2017.

[21] F. Clazzer, A. Munari, G. Liva, F. Lazaro, C. Stefanovic, and P. Popovski, "From 5G to 6G: Has the time for modern random access come?" 2019. [Online]. Available: https://arxiv.org/abs/1903.03063.

[22] S. Alvi, S. Durrani, and X. Zhou, "Enhancing CRDSA with transmit power diversity for machine-type communication," *IEEE Trans. Veh. Technol.*, vol. 67, no. 8, pp. 7790–7794, Aug. 2018.

[23] X. Shao, Z. Sun, M. Yang, S. Gu, and Q. Guo, "NOMA-based irregular repetition slotted ALOHA for satellite networks," *IEEE Commun. Lett.*, vol. 23, no. 4, pp. 624–627, Apr. 2019.

[24] X. Ge, J. Yang, H. Gharavi, and Y. Sun, "Energy efficiency challenges of 5G small cell networks," *IEEE Commun. Mag.*, vol. 55, no. 5, pp. 184–191, May 2017.

[25] D. H. Gultekin and P. H. Siegel, "Absorption of 5G radiation in brain tissue as a function of frequency, power and time," *IEEE Access*, vol. 8, pp. 115593–115612, 2020.

[26] F. Babich and M. Comisso, "Segmented framed slotted Aloha (SFSA) with capture and interference cancellation," in *Proc. IEEE 87th Veh. Technol. Conf. (VTC Spring)*, Porto, Portugal, 2018, pp. 1–5.

[27] M. Comisso and F. Babich, "Coverage analysis for 2D/3D millimeter wave peer-to-peer networks," *IEEE Trans. Wireless Commun.*, vol. 18, no. 7, pp. 3613–3627, Jul. 2019.

[28] T. Bai and R.W. Heath Jr., "Coverage and rate analysis for millimeter-wave cellular networks," *IEEE Trans. Wireless Commun.*, vol. 14, no. 2, pp. 1100–1114, Feb. 2015.

[29] F. Babich and M. Comisso, "Impact of header on coded slotted Aloha with capture," in *Proc. IEEE Symp. Comput. Commun. (ISCC)*, Barcelona, Spain, 2019, pp. 1–6.

[30] F. Clazzer, E. Paolini, I. Mambelli, and Č. Stefanović, "Irregular repetition slotted ALOHA over the Rayleigh block fading channel with capture," in *Proc. IEEE Int. Conf. Commun. (ICC)*, Paris, France, 2017, pp. 1–6.

[31] F. Clazzer, C. Kissling, and M. Marchese, "Enhancing contention resolution ALOHA using combining techniques," *IEEE Trans. Commun.*, vol. 66, no. 6, pp. 2576–2587, Jun. 2018.

[32] F. Babich and M. Comisso, "Impact of segmentation and capture on slotted ALOHA systems exploiting interference cancellation," *IEEE Trans. Veh. Technol.*, vol. 68, no. 3, pp. 2878–2892, Mar. 2019.

[33] A. Mengali, R. De Gaudenzi, and Č. Stefanović, "On the modeling and performance assessment of random access with SIC," *IEEE J. Sel. Areas Commun.*, vol. 36, no. 2, pp. 292–303, Feb. 2018.

[34] A. Mengali, R. De Gaudenzi, and P. D. Arapoglou, "Enhancing the physical layer of contention resolution diversity slotted ALOHA," *IEEE Trans. Commun.*, vol. 65, no. 10, pp. 4295–4308, Oct. 2017.

[35] F. Babich, G. Buttazzoni, F. Vatta, and M. Comisso, "Energy-constrained NOMA with packet diversity for slotted ALOHA systems," in *Proc. IEEE Mediterranean Commun. Comput. Netw. Conf. (MedComNet)*, Arona, Italy, 2020, pp. 1–8.

[36] F. Babich and A. Crismani, "Cooperative coding schemes: Design and performance evaluation," *IEEE Trans. Wireless Commun.*, vol. 11, no. 1, pp. 222–235, Jan. 2012.

[37] P. Kota and C. Schlegel, "A wireless packet multiple access method exploiting joint detection," in *Proc. IEEE Int. Conf. Commun. (ICC)*, Anchorage, AK, USA, 2003, pp. 2985–2989.

[38] J. G. Andrews and T. H. Meng, "Optimum power control for successive interference cancellation with imperfect channel estimation," *IEEE Trans. Wireless Commun.*, vol. 2, no. 2, pp. 375–382, Mar. 2003.

[39] A. Agrawal, J. G. Andrews, J. M. Cioffi, and T. H. Meng, "Iterative power control for imperfect successive interference cancellation," *IEEE Trans. Wireless Commun.*, vol. 4, no. 3, pp. 878–884, May 2005.